Electrochimica Acta 343 (2020) 136121

Contents lists available at ScienceDirect

Electrochimica Acta

journal homepage: www.elsevier.com/locate/electacta

Sandwich-like dual carbon layers coated NiO hollow spheres with superior lithium storage performances

Qingmeng Gan [a, b, *, 1], Buchen Wu [a, b, 1], Ning Qin [b, c], Jiali Chen [a, b], Wen Luo [b], Dejun Xiao [a], Jie Feng [d], Weilong Liu [a], Youhuan Zhu [b], Peisen Zhang [e]

[a] Department of Mechanical Engineering, National University of Singapore, 117575, Singapore
[b] Department of Materials Science and Engineering, Guangdong Provincial Key Laboratory of Energy Materials for Electric Power, Southern University of Science and Technology, Shenzhen, 518055, China
[c] Department of Mechanical Engineering, City University of Hong Kong, 83 Tat Chee Avenue, Hong Kong, 999077, China
[d] School of Civil Engineering, Harbin Institute of Technology, 150001, China
[e] Key Laboratory of Colloid, Interface and Chemical Thermodynamics, CAS Research/Education Center for Excellence in Molecular Sciences, Institute of Chemistry, Chinese Academy of Sciences, Beijing, 100190, PR China

ARTICLE INFO

Article history:
Received 4 January 2020
Received in revised form
14 March 2020
Accepted 22 March 2020
Available online 29 March 2020

Keywords:
Dual carbon later coating
Sandwich-like structure
Hollow sphere
Outstanding cycling stability
First principle theory

ABSTRACT

Transition metal oxides (e.g. NiO) have been considered as promising high-capacity anode in lithium ion batteries (LIBs). However, the low electronic conductivity and huge volume change during cycling lead to rapid capacity fading and poor rate capability. To solve those drawbacks, we design a sandwich-like dual carbon layers coated hollow structured NiO (C@NiO@NC). The NiO nanosheets are anchored on the surface of hollow carbon nanospheres and then coated with N-doped porous carbon layer, which confine them between two carbon shells. Such hierarchical architecture with high surface area increases the contact between the electrode and electrolyte, resulting in decreased Li^+ diffusion pathway. Moreover, the dual carbon layers enhance the electronic conductivity of C@NiO@NC and effectively buffer the volume changes of NiO during cycling. Therefore, this sample delivers a high capacity (1189 mA h g^{-1} at 100 mA g^{-1}), superior rate capability (420 mA h g^{-1} at ultrahigh rate of 10000 mA g^{-1}) and outstanding cycling stability (96.1% at 1000 mA g^{-1} after 1000 cycles) when used as LIBs anode. The density functional theoretical calculation further proves the enhanced electronic conductivity and more energetic favorable capability of C@NiO@NC. This facile method can be extended to other transition-metal oxides with superior electrochemical performance.

© 2020 Elsevier Ltd. All rights reserved.

1. Introduction

Transition metal oxides (e.g., NiO[1–3], SnO_2[4,5], Fe_2O_3[6,7] and Co_3O_4[8,9]) are promising candidates to replace commercial graphite anode in lithium ion batteries (LIBs) due to their high theoretical capacity. Among various transition metal oxides anodes, NiO has been widely studied as a high-energy LIBs anode because of its high theoretical capacity (718 mA h g^{-1}), low toxicity as well as low cost[10–12]. Nevertheless, the practical application of NiO has been dramatically restricted by the serious volume expansion upon lithiation/delithiation process, leading to high pulverization and rapid capacity fading. Besides, the exposure of fresh surface of the active materials caused by the huge volume change during cycling would lead to continuous formation of solid electrolyte interface (SEI) film. The formation of thick SEI film on the surface would slow down the Li^+ diffusion kinetics and elongate Li^+ diffusion path. Moreover, the relatively poor electrical conductivity of NiO is somewhat unsatisfactory because it can largely affect the rate performance[13,14].

In the past few years, various strategies have been developed to solve the above drawbacks. One effective way is to design the active materials with specific morphologies, including microspheres[15], rod-in-tube [16], nanorods[17], nanodots[18]. Through particular morphology design, the Li^+ transport path length is largely shortened and the mechanical strain during cycling is better buffered, leading to promoted cycling stability. Another effective way is combining transition metal oxide with conductive carbon matrix,

* Corresponding author. Department of Mechanical Engineering, National University of Singapore, 117575, Singapore.
E-mail addresses: qingmenggan@u.nus.edu, qingmenggan@126.com (Q. Gan).
[1] These authors contributed equally.

https://doi.org/10.1016/j.electacta.2020.136121
0013-4686/© 2020 Elsevier Ltd. All rights reserved.

which can not only protect the active material from reacting with the electrolyte but also increase the electronic conductivity. Moreover, our previous works and abundant reported references have proved that the volume expansion of oxide mental oxides could be alleviated with carbon coating during lithiation/delithiation process[19–22]. For example, Wang's group encapsulated peapod-like NiO nanoparticles into carbon fibers to promote the ion diffusion kinetics and restrain the volume changes upon long-time reactions[23]. Our group reported enhanced electronic conductivity and superior cycling stability of FeO_x nanoparticles with N-doped porous carbon coating[24]. Inspiration from the above discussions, it can be forecasted that morphology designing combined with uniform and tight carbon coating would be a promising approach to enhance the electrochemical performance for transition metal oxides.

Recently, extensive attention has been focused on developing carbon supported or carbon coated hollow structured transition metal oxide. The hollow structure with large surface area could endow sufficient soaking of electrolyte, largely facilitating Li^+ diffusion kinetics due to the shortened ion diffusion length. In the case of carbon supported transition metal oxides, the carbon matrix can serve as continuous electronic conductive high way and alleviate the volume change of active material to some extent. However, the transition metal oxide wrapped outside is easy to be pulverized and detached from the carbon matrix during repeated lithiation-delithiation process due to the absence of surface protection layer. This situation will lead to the continuous formation of thick and rough SEI film, which subsequently cause poor electronic conduction on the surface of active material. The surface coating layer can provide good surface electronic conduction and accommodate the expansion of active materials without destroying the protection carbon layers on the surface. However, the inner side active materials still suffer high mechanical stress, thus promoting the tendency of cracking and crumbling, resulting in unsatisfactory cycling stability. Accordingly, synthesizing hollow structured transition metal oxide with dual carbon coating layers could enhance the electronic conductivity, stabilize the surface SEI film and alleviate structure cracking during cycling, consequently improving the electrochemical performance.

In this work, we fabricated a sandwich-like dual carbon layers coated NiO hollow sphere (denoted as C@NiO@NC) by using polystyrene sphere as template. In this unique architecture, the NiO nanosheet, which is assembled by ultrasmall NiO nanoparticles (~10 nm), were anchored vertically on the surface of hollow carbon and then coated with a nitrogen-doped carbon layer outside the particles. The sandwich-like structure well confined the NiO nanoparticles between the two carbon layers, which can obviously enhance the electronic conductivity of active materials. The interstitial void space between the active materials and carbon layers can serve as a cushion to buffer the volume expansion of NiO without breaking the carbon layers upon charge-discharge process. Also, the stable dual carbon layers allow for the growth of a stable SEI film on the carbon shell surface, resulting in decreased irreversible capacity and capacity fading. Besides, the ultrasmall NiO nanoparticles integrated with the surrounded electronically and ionically conductive carbon can ensure fast electron transport and ion diffusion in the overall electrode. As an anode for LIBs, C@NiO@NC shows a high reversible capacity (1189 mA h g^{-1} at 100 mA g^{-1}), superior rate capability (420 mA h g^{-1} at ultrahigh rate of 10000 mA g^{-1}) as well as excellent cycling stability (capacity retention of 96.1% at 1000 mA g^{-1} after 1000 cycles). Density functional theory (DFT) calculations further reveals the increased electrical conductivity and lower energy barriers of the lithiation process of C@NiO@NC.

2. Experimental section

2.1. Preparation of sulfonated polystyrene nanospheres (SPS)

Polystyrene nanospheres (PS) were synthesized based on our previous work[25]. After drying the emulsion at 60 °C, the white PS powder was obtained. Sulfonated polystyrene was prepared by a simple solution method. In detail, white PS powder (2 g) was poured into concentrated sulfuric acid (polystyrene: H_2SO_4 = 1: 30, w/w). The mixture was stirred at 40 °C for 30 min to fully sulfurate the PS powder. Finally, the pinkish sulfonated polystyrene nanospheres (SPS) was collected by centrifugation and washed thoroughly with water and ethanol[26,27].

2.2. Preparation of SPS@Ni-precursor

500 mg of $Ni(NO_3)_2 \cdot 6H_2O$ and 150 mg of hexamethylenetetramine were dissolved into 200 mL of 0.7 mM trisodium citrate solution. Then, 100 mg of SPS was dispersed into the mixture through sonication for 20 min. After that, the mixture was transferred into a 500 mL three-necked flask and stirred at 90 °C for 10 h. The green precipitate was washed thoroughly with ethanol for three times, and dried at 60 °C for 12 h.

2.3. Preparation of sandwich-like dual carbon layers coated NiO hollow sphere nanostructures (C@NiO@NC)

Initially, SPS@Ni-precursor (300 mg) was dispersed into Tris buffer solution (50 mL, pH = 8.5) by sonication for 15 min. Then, dopamine hydrochloride (50 mg) was added into the mixture. After stirring at 30 °C for 3 h, the yellow powder (SPS@Ni-precursor@PDA) was collected after washing with ethanol for three times by centrifugation. To obtain C@NiO@NC, the SPS@Ni-precursor@PDA powder was sintered at 500 °C for 2 h under Ar atmosphere. For comparison, C@NiO was obtained by sintering SPS@Ni-precursor following the same process as C@NiO@NC.

2.4. Characterizations

X-ray diffraction (XRD) patterns were obtained through using a Rigaku D/Max-2400 X-ray diffractometer (Cu Kα, λ = 0.15405 nm). The morphologies of active materials were collected by the scanning electron microscopy (SEM, TESCAN MIRA3, 20 kV) and transmission electron microscopy (TEM, JEOL JEM-2100, 300 kV). X-ray photoelectron spectroscopy (XPS) was taken on a Thermo ESCALAB 250Xi XPS spectrometer (Al Kα, 1486.6 eV). Thermogravimetric analysis (TGA) data was obtained through utilizing a Mettler-Toledo TGA DSC 1 Star^e system. N_2 adsorption-desorption isotherms was obtained through using a Builder SSA-4200 instrument.

2.5. Electrochemical measurements

Electrochemical testing was performed by utilizing 2016 coin-type cells. Anode was composed of active materials, polyvinylidene fluoride (PVDF), and super P (8:1:1 w/w/w) by using *N*-methyl-2-pyrrolidone (NMP) as solvent. The slurry was coated onto a copper foil. 1 M $LiPF_6$ in dimethyl carbonate/ethylene carbonate/ethyl methyl carbonate (1:1:1 v/v/v) was used as electrolyte. Galvanostatic charge-discharge was tested on a Neware battery testing system (CT-3008W, 0.01–3.0 V vs Li/Li^+) at room temperature. Cyclic voltammetry (CV, 0.01–3.0 V) and electrochemical impedance spectroscopy (EIS, frequency range: 100 kHz-10 mHz) were recorded on an electrochemical workstation (BioLogic-VMP3).

2.6. Calculation methods

Density functional theory (DFT) calculations were carried out through implementing Material Studio software. To accurately calculate the electrical conductivity and energy barriers of the lithiation process, Perdew-Burke-Ernzerhof function generalized gradient approximation with the method of CASTEP. The energy cutoff of a plane-wave is 370 eV to ensure the precision of the calculations. For calculations of the electronic properties and equilibrium geometries, the integrations over the Brillouin zone were carried out with a $3 \times 3 \times 3$ k-point grid.

3. Results and discussion

Fig. 1 shows the synthesis process of the sandwich-like dual carbon layers coated C@NiO@NC hollow spheres. The sulfonic acid ($-SO_3^-H^+$) groups enriched polystyrene sphere (SPS) is used as template. Firstly, the Ni^{2+} is absorbed on the surface of SPS through the electrostatic interaction between the sulfonic acid groups and Ni^{2+}, which promotes the growth of nanosheet-like Ni-precursor and form the SPS@Ni-precursor[26]. Ni-precursor should be $Ni(OH)_2$ particles and then assemble NiO nanosheets through treatment at high temperature (proved by the following TEM images). After that, dopamine monomer polymerize to a continuous polymer layer on the surface of the SPS@Ni-precursor during the oxidization and cyclization reaction owing to the strong binding affinity between Ni^{2+} and the −OH from dopamine monomer [28]. Then, the SPS and the PDA are decomposed and released a little gas (e.g., methane, ethylene, propylene and CO_2) at high temperature. Finally, the SPS@Ni-precursor@polydopamine is transformed into sandwich-like dual carbon layers coated C@NiO@NC nanostructure. The inside carbon layer came from the carbonization of SPS, while outer carbon layer originated from PDA.

The structures and morphologies of as-prepared materials are characterized by scanning electron microscopy (SEM) and transmission electron microscopy (TEM). As shown in Fig. 2a and b, the pristine PS nanospheres exhibit high uniformity with a diameter of ~1 μm and smooth surface. The C@NiO shows a hollow sphere morphology, which is assembled from NiO nanosheets (Fig. 2c and d). As seen, under the assistance of $-SO_3^-H^+$ groups, Ni^{2+} ions are easy to absorb on the surface of SPS nanospheres because of the electrostatic interaction and grow to uniform nanosheet under the reaction. After coating N-doped carbon layer, the NiO nanosheets become thick, signifying the successful introduction of carbon layer outside the surface of NiO nanosheets. The TEM images (Fig. 2g−h) illustrate the hollow sphere structure of C@NiO@NC. From the magnified TEM images (Fig. 2i), it can be observed that the NiO nanosheets are assembled by ultrasmall NiO nanoparticles (~10 nm) and are completely wrapped with N-doped carbon. HRTEM images (Fig. 2j) of C@NiO@NC shows interplanar spacing of 0.24 nm, assigning to the (111) facet of face-centered cubic NiO phase. The inside selected-area electron diffraction (SAED) pattern of the C@NiO@NC shows four intense rings indexed to the (111), (200), (220), and (311) crystal planes of crystalline NiO phase. Based on the elemental mapping analysis (Fig. S1), it is clear that the presence of carbon (C), oxygen (O), nitrogen (N), and nickel (Ni) in C@NiO@NC. As shown, C and N elements uniformly distribute around Ni element, indicating the successfully synthesis of sandwich-like dual carbon layers coated NiO hollow spheres.

The crystalline phase of hollow C@NiO and C@NiO@NC nanospheres are characterized by XRD patterns. As exhibited in Fig. 3a, four well-defined diffraction peaks at 37.2°, 43.3°, 62.9°, and 75.4° are corresponding to (111), (200), (220), and (311) crystal phase of NiO (JCPDS No. 47−1049) [29,30], respectively, matching well with the above mentioned SAED pattern. Using Scherrer equation ($D = k\lambda/\beta\cos\theta$, β is the half-peak width of the diffraction peak profile at maximum diffraction peak, where k is a constant normally used 0.9) with the broadening of the (2 0 0) peaks, the crystal sizes along the [2 0 0] direction for C@NiO and C@NiO@NC are calculated to be 12.1 and 13.6 nm, respectively, corresponding to the size of TEM images. The XPS survey spectra (Fig. 3b) for both C@NiO and C@NiO@NC show similar peaks of C 1s, O 1s and Ni 2p, while the N 1s peak only appears in C@NiO@NC, demonstrating the successful incorporation of nitrogen-doped carbon layers. As shown in the N 1s spectrum of C@NiO@NC (Fig. 3c.), three peaks at 398.5, 400.9 and 403.1 eV can be assigned to pyridinic nitrogen (N-6), pyrrolic nitrogen (N-5), and quaternary nitrogen (N-Q), respectively [31,32]. Through calculation, the N content (related to carbon layer) in C@NiO@NC is about 3.5 wt%, which can provide extra unpaired electrons, and thus improve carrier concentration. Therefore, the electronic conductivity of C@NiO@NC is greatly improved[24,33,34]. The presence of C−N peak in high-resolution C 1s XPS spectrum of C@NiO@NC further proves the existence of N in the outer carbon layer (Fig. S2a). As for Ni 2p spectra, the Ni^{2+} peaks

Fig. 1. Schematic illustration of the synthesis process of C@NiO@NC.

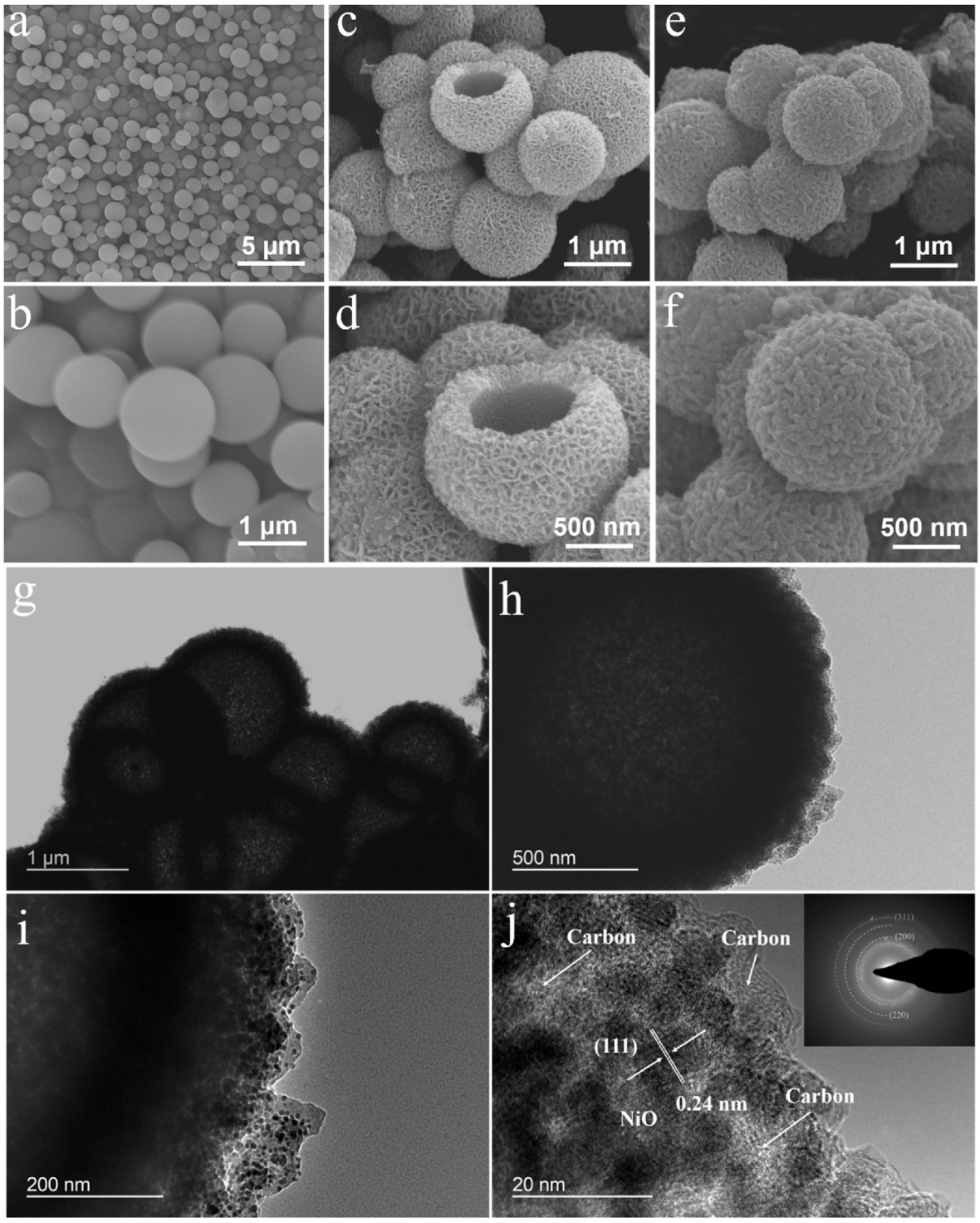

Fig. 2. SEM images of (a and b) PS nanospheres, (c and d) C@NiO, and (e and f) C@NiO@NC. (g–i) TEM and (j) HRTEM images for C@NiO@NC (the inset is SEAD image for C@NiO@NC).

at 852.6 and 870.2 eV dominate the largest proportion, indicating the metal oxides is mainly NiO (Fig. 3d). As shown in Fig. S2b, both two samples possess the bonds of Ni–CO_3 and C–O, while the Ni–O bond is only observed in C@NiO[35]. This phenomenon is ascribed to the existence of outer nitrogen-doped carbon layer for C@NiO@NC, which completely coats the surface of NiO and thus covers the inside Ni–O bonds.

N_2 adsorption-desorption isotherm was utilized to investigate the surface area and porous property of C@NiO@NC. As shown in Figs. 3e and S3, the N_2 adsorption-desorption isotherm of both samples are typical type IV isotherm with an obvious H3 hysteresis loop, indicating the existence of mesopores in C@NiO@NC and C@NiO composites. Indeed, based on the Barrett-Joyner-Halenda (BJH) method, the corresponding pore-size distributions of C@NiO is mainly 3.84 nm. As for C@NiO@NC, the pore sizes are mainly at 3.78 and 6.92 nm. The additional mesopores of

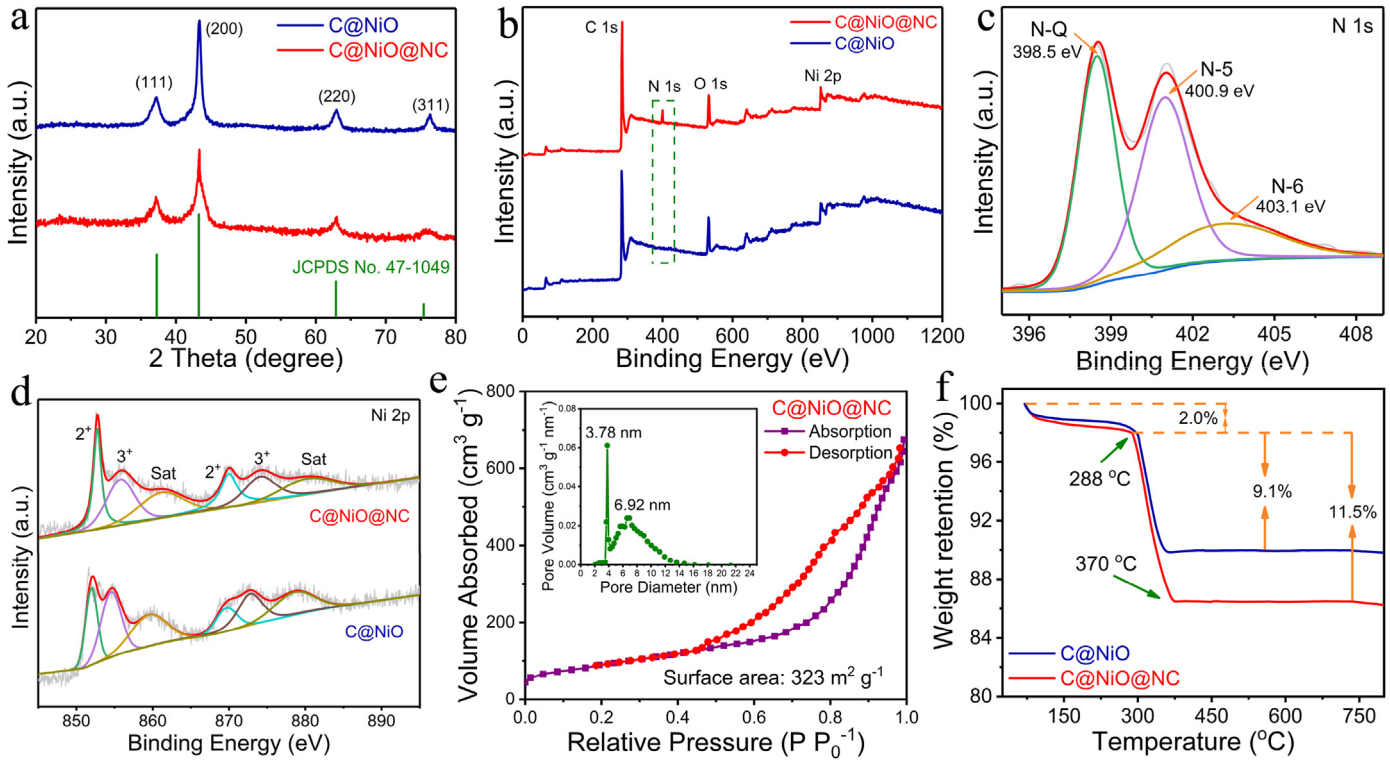

Fig. 3. (a) XRD patterns of C@NiO and C@NiO@NC. (b) XPS survey spectra of C@NiO and C@NiO@NC. (c) High-resolution N 1s XPS spectrum of C@NiO@NC. (d) High-resolution Ni 2p XPS spectra of C@NiO and C@NiO@NC. (e) N_2 adsorption-desorption isotherm and corresponding BJH pore size distribution of C@NiO@NC. (f) TGA curves of C@NiO and C@NiO@NC.

C@NiO@NC mainly come from the out N-doped porous carbon layer. The BET specific surface area for C@NiO@NC is up to 323 $m^2 g^{-1}$, which is much higher than that of C@NiO (225 $m^2 g^{-1}$). The high surface area can provide efficient electrolyte soaking and abundant active sites for electrochemical reactions during cycling, while mesopores properties of C@NiO@NC nanospheres can facilitate the diffusion of Li^+ between electrolyte and anode. According to TGA results (Fig. 3f), the carbon contents of C@NiO and C@NiO@NC composites are 9.1% and 11.5%, respectively, suggesting that NiO is the principal component in both samples.

To investigate the superiority of the sandwich-like dual carbon layers coated structure, the lithium storage performance for C@NiO and C@NiO@NC were tested. The cycling performance of C@NiO and C@NiO@NC at 100 mA g^{-1} are displayed in Fig. 4a. As seen, C@NiO@NC shows an initial Coulombic efficiency of 79.5% with a capacity up to 1189 mA h g^{-1} after 200 cycles, which is much higher than that of C@NiO (67.2%, 758 mA h g^{-1}). This result suggests that the out N-doped porous carbon can provide more active sites for electrochemical reaction, leading to much higher capacity. The higher initial coulombic efficiency of C@NiO@NC is ascribed to the outside carbon layer coated on C@NiO@NC that largely avoid the detrimental reactions between NiO and electrolyte. The loss of initial irreversible capacity could be assigned to the inevitable formation of the SEI layer and decomposition of the electrolyte [20,36]. Moreover, the protection of outer N-doped porous carbon layer can block the direct contact between electrolyte and anode material, ensure the formation of stable and thin SEI film, and thus reduce the side reaction and increase the cycling stability[37]. After the initial cycle, the C@NiO@NC only needs 4 cycles to reach nearly 100% Coulombic efficiency, while C@NiO needs 9 cycles. Besides, the capacities of both anodes show increased tendency. However, the capacity of C@NiO@NC increases at about 50th cycle, while that of C@NiO enhance at around 150th cycle. The capacities increased tendency is ascribed to the activation process of NiO, which is a common phenomenon in metal oxides[26,35]. The faster activation process for C@NiO@NC is assigned to the outer porous carbon layer, which can facilitate the diffusion of Li ions. The corresponding galvanostatic charge-discharge profiles for C@NiO@NC and C@NiO at various cycles are illustrated in Figs. 4c and S4a. As seen, C@NiO@NC shows well-defined plateau with small polarization during charge-discharge process, while the C@NiO electrode have no obvious plateaus but serious polarization, indicating better reaction reversibility and cycling stability of C@NiO@NC.

Rate performance is an important parameter to evaluate the electrochemical property of C@NiO@NC. As shown in Fig. 4d, C@NiO@NC displays reversible capacities of 1189, 1003, 899, 757, and 659 mA h g^{-1} at 100, 200, 500, 1000, and 2000 mA g^{-1}, respectively. Interestingly, even at ultrahigh rates of 5000 and 10000 mA g^{-1}, C@NiO@NC anode can still hold capacities of 510 and 420 mA h g^{-1}, respectively. As a contrast, C@NiO anode only shows capacities of 370 and 199 mA h g^{-1} at high rates of 5000 and 10000 mA g^{-1}. The corresponding charge-discharge profiles of C@NiO@NC maintains well at various current rates, while those for C@NiO exhibit severe deformation at high rates (Figs. 4e and S4b). The excellent rate performance of C@NiO@NC can be assigned to the facilitated Li^+ diffusion kinetics originated from the unique sandwich-like dual carbon layers coated hollow structure. To evaluate the stability of the unique sandwich-like dual carbon layers coated hollow structure for C@NiO@NC, long-term cycling performance was investigated at 1000 mA g^{-1} over 1000 cycles. As shown in Fig. 4g, it delivers a very high capacity of 832 mA h g^{-1} at 1000 mA g^{-1} with a capacity retention of 96.1% after 1000 cycles. For comparison, C@NiO anode only shows a poor capacity retention of 36.8%. In order to further highlight the outstanding cycling stability and rate performance of C@NiO@NC, we compared the electrochemical performance of the C@NiO@NC with previously

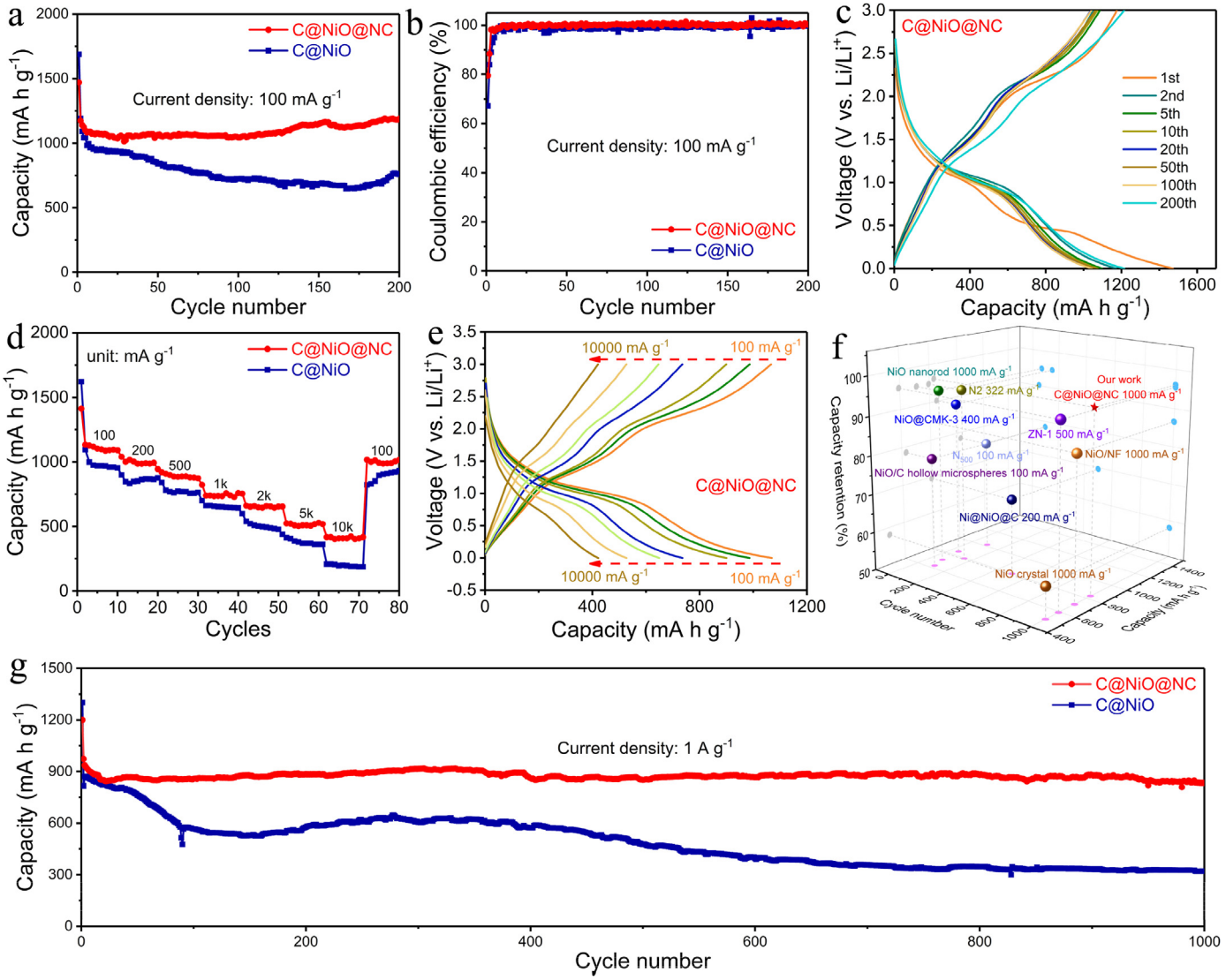

Fig. 4. (a) Cycling performance of C@NiO and C@NiO@NC at 100 mA g^{-1}, (b) corresponding Coulombic efficiency and (c) charge-discharge profiles of C@NiO@NC at various cycles. (d) Rate performance of C@NiO and C@NiO@NC and (e) corresponding charge-discharge profiles at different rates. (f) Comparison of the high-rate cycling performance of C@NiO@NC anode with other reported Ni-based anodes of LIBs. (g) Long-term cycling performance of C@NiO and C@NiO@NC at 1000 mA g^{-1} over 1000 cycles.

reported NiO-based anode materials with various structures (Fig. 4f and Table S1). Obviously, the unique sandwich-like dual carbon layers coated hollow structured C@NiO@NC in this work exhibit much better cycling stability and rate performance compared to other structured NiO-based anodes, including NiO nanodots[11], NiO nanosheets[38], NiO/C hollow microspheres [15], NiO nanorod [39], Ni@NiO nanocomposites [40], yolk-shell ZnO/NiO microspheres [41], mesoporous NiO nanorod[14], mesoporous NiO crystals [42], and 3D-NiO microspheres [43].

EIS are tested to evaluate the charge transfer resistance and ion diffusion resistance of both electrode materials. The equivalent circuit diagram for fitting is shown in Fig. S5. As seen, both samples show a semicircle at high frequency range and a slope at low frequent range, which are represent for the charge transfer resistance and ion diffusion resistance, respectively[44]. After the activation process during initial cycles, the C@NiO@NC (102 Ω) electrode shows much lower charge transfer resistance ($R_{(sf+ct)}$) than that of C@NiO (145 Ω), indicating increased electronic conductivity after the N-doped carbon coating, which is in good agreement with the excellent rate performance of C@NiO@NC (Fig. 5a and b). The structure collapsing would cause the continues formation of SEI film, resulting in poor contact between the electrode with the electrolyte thus affecting the charge transfer resistance and the ion diffusion kinetics[17,33]. Therefore, the EIS curves after various cycles were measured to further evaluate the structure stability of C@NiO@NC and C@NiO. As shown in Fig. 5a and b, both electrodes illustrate similar tendency upon cycling. Initially, the $R_{(sf+ct)}$ becomes lower at the initial several cycles ascribing to the activated process. Then, it increases with the increasement of the cycling number because of the structure collapsing of both electrodes. As comparison, the value of $R_{(sf+ct)}$ for C@NiO (131 Ω) is much higher than that of C@NiO@NC (258 Ω) after 200 cycles. This result suggests that the structure of C@NiO@NC is better preserved upon cycling compared to the C@NiO. Moreover, the slope for the C@NiO@NC electrode after 200 cycles is much higher than that of C@NiO, indicating better ion diffusion kinetics, which may due to the formed stable and thin SEI film at the surface owing to the well preserved structure, better interfacial contact between the electrode and electrolyte and highly improved electronic conductivity. To give a directly observation of the structure change during

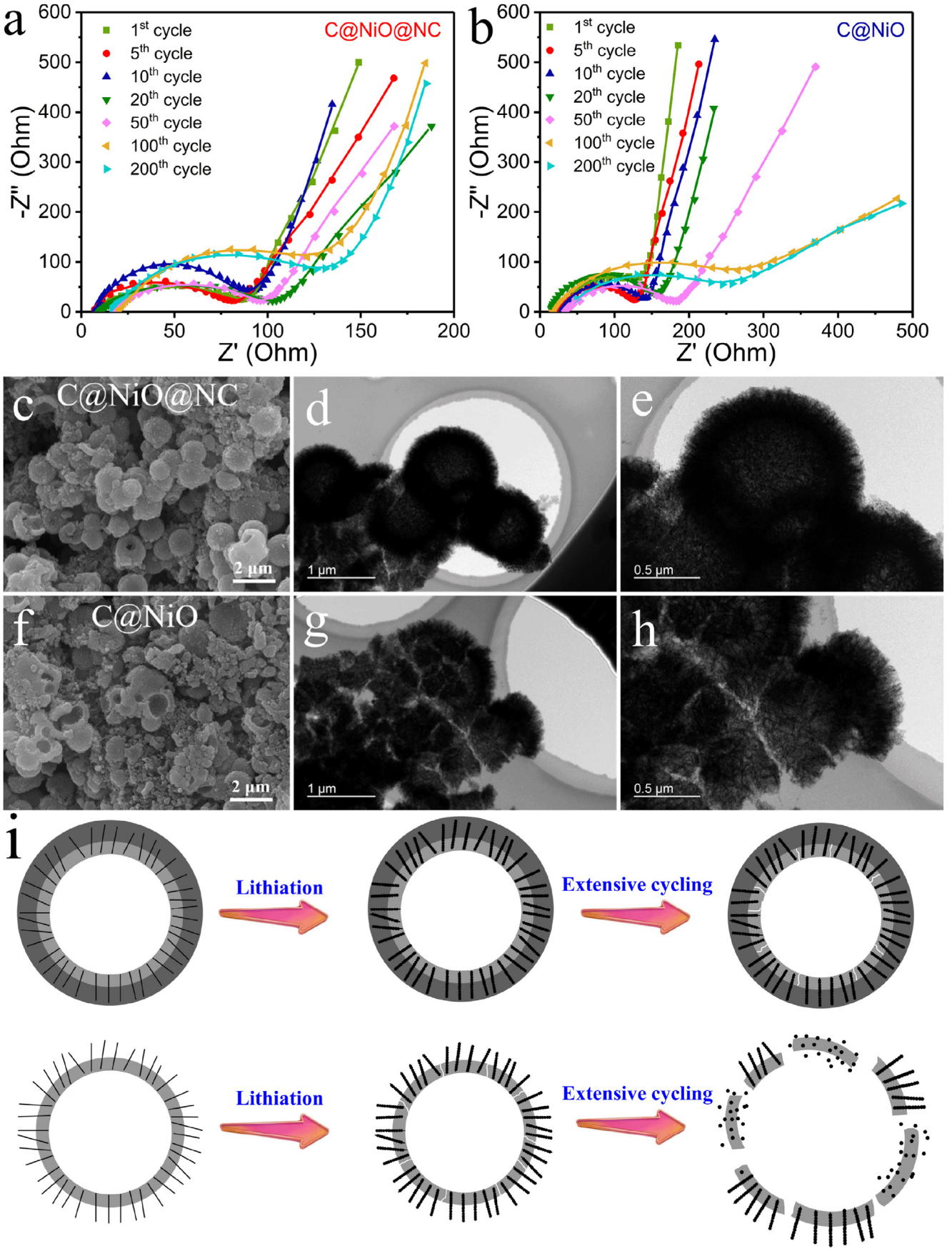

Fig. 5. EIS curves of (a) C@NiO@NC and (b) C@NiO anodes at different cycles. Cycled SEM images of (c) C@NiO@NC and (f) C@NiO after 50 cycles. Cycled TEM images of (d and e) C@NiO@NC and (g and h) C@NiO after 50 cycles. (i) Schematic illustration of the lithiation process and repeated cycles of C@NiO@NC and C@NiO.

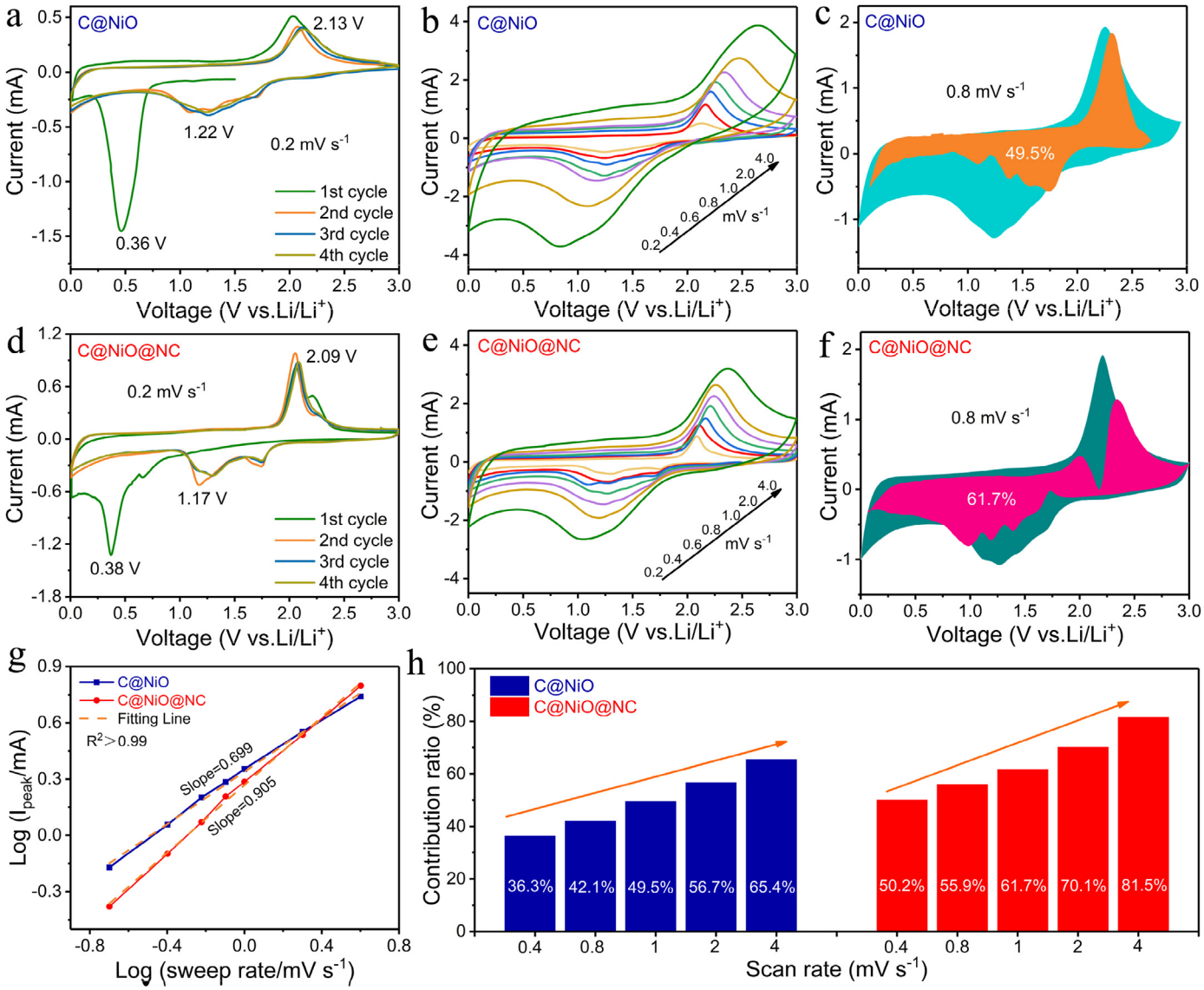

Fig. 6. CV curves of (a) C@NiO and (b) C@NiO@NC at 0.2 mV s^{-1}. CV curves at various scan rates from 0.2 to 4 mV s^{-1} of (a) C@NiO and (b) C@NiO@NC. Capacitive and diffusion-controlled contribution of (c) C@NiO and (f) C@NiO@NC at 0.8 mV s^{-1}. (g) Log *i* vs log *v* plots. (h) Normalized contribution ratios of capacitive capacities at different scan rates.

cycling, the SEM and TEM images for both electrodes after 50 cycles were collected. As shown in Fig. 5c–e, the sandwich-like hollow structure of C@NiO@NC can maintain well without obvious structure collapsing, however, C@NiO without the outer side protection carbon layer trends to crack after 50 cycles (Fig. 5f–h). Owing to the above results, the corresponding morphologies change of C@NiO@NC and C@NiO upon cycling can be depicted in Fig. 5i. As shown, sandwich-like dual carbon layers coated NiO exhibits great performance and long cycling stability, such that it markedly outperforms C@NiO. These phenomena clearly demonstrate the outstanding stability of the unique sandwich-like dual carbon layers coated hollow structure of C@NiO@NC.

CV was measured to investigate the electrochemical reaction of anodes during charge-discharge process. As shown in Fig. 6a and d, in the first cycle, both electrodes show a cathodic peak at about 0.36 V, corresponding to the initial reduction of NiO to Ni ($NiO + 2Li^+ + 2e^- \rightarrow Ni + Li_2O$), along with the irreversible formation of amorphous Li_2O and decomposition of electrolyte to form solid electrolyte interface (SEI) film [26,43]. At the initial cathodic process, a broad oxidation peak appears in both samples, assigning to the oxidation of metallic Ni to nanosized NiO ($Ni + Li_2O \rightarrow NiO + 2Li^+ + 2e^-$)[10,41]. During the subsequent cycles, a pair of redox peaks at 1.17/2.09 V for C@NiO@NC and 1.22/2.13 V C@NiO are observed. Smaller voltage deviation for C@NiO@NC indicates better reversibility for the unique sandwich-like dual carbon layers coated hollow structure. Better overlap of CV curves for C@NiO@NC is demonstrated, revealing better cycling stability during cycling.

To deeply reveal the underlying reason responsible for the superior electrochemical performance, the kinetic study of C@NiO and C@NiO@NC anode was discussed through CV curves at various scan rates. Fig. 6b and e displays the CV curves at different sweep rates from 0.2 to 4.0 mV s^{-1}. Compared with C@NiO, the C@NiO@NC exhibits much smaller polarization as sweep rate increases, suggesting the rapid charge-transfer process. According to the previous references, it is well known that the Li^+ storage mechanism consists of capacitive and diffusion dominated process, which can be revealed based on the following Eqs. (1) and (2) [45,46]:

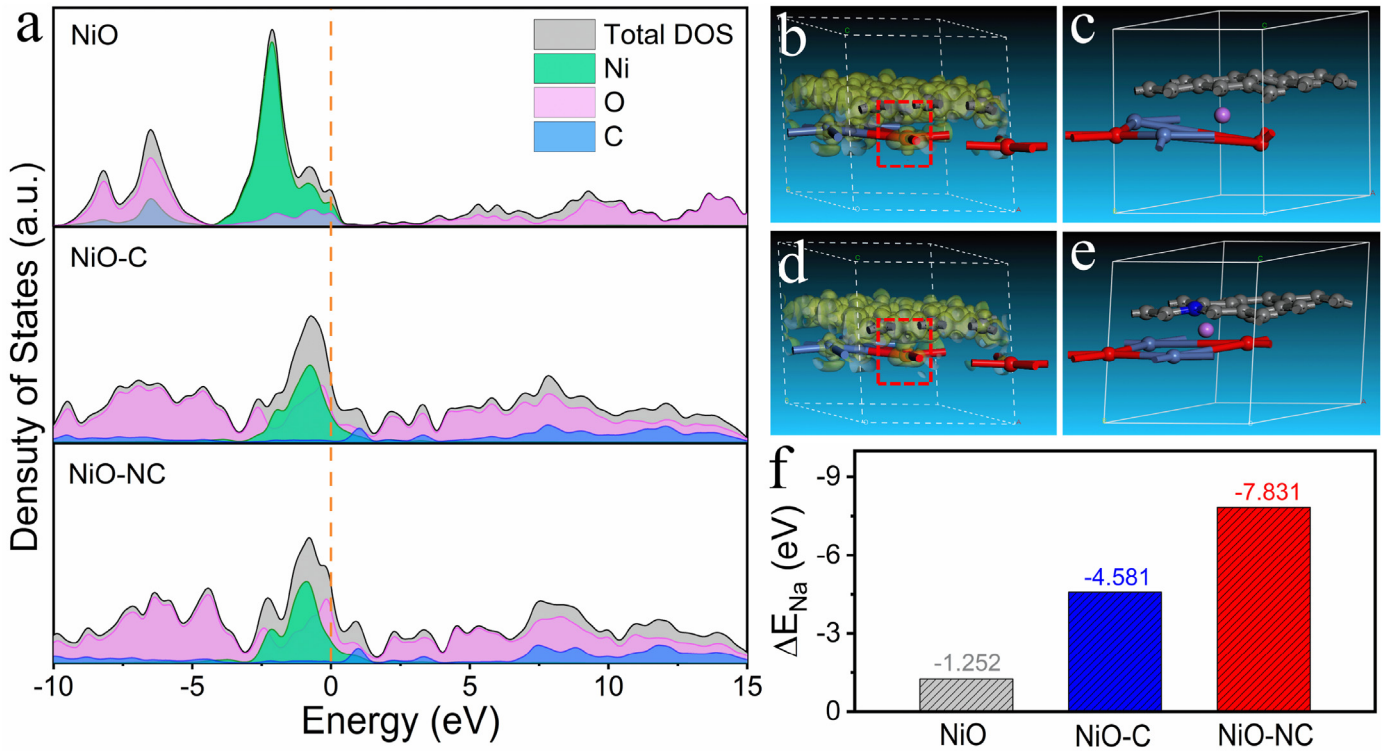

Fig. 7. (a) Calculated density of states of Pristine NiO, NiO−C, and NiO-NC. The computed differential charge density of (b) NiO−C and (d) NiO-NC; yellow bubbles stand for the electron accumulation. The computed Li^+ intercalation models for the (c) NiO−C, (e) NiO-NC. (f) Calculations of the Li^+ adsorption energy of NiO, NiO−C, and NiO-NC. (For interpretation of the references to colour in this figure legend, the reader is referred to the Web version of this article.)

$$i = av^b \quad (1)$$

$$\log(i) = b\log(v) + \log(a) \quad (2)$$

In these equations, *i* and *v* are current and scan rate, respectively, while a and b are adjustable parameters. b = 1 stands for that the Li^+ storage is fully dominated by a capacitive process, while b = 0.5 stands for a fully diffusion dominated process. The calculation results are depicted in Fig. 6g. The slope (the value of b) of C@NiO@NC is up to 0.905, much larger than that of C@NiO (0.699), indicating the optimized capacitive kinetics of C@NiO@NC. In detail, the contribution of capacitive and diffusion-controlled reaction is further quantitatively investigated on the basis of the following Eq. (3)[25, 47]:

$$i(V) = k_1 v + k_2 v^{1/2} \quad (3)$$

As shown in Fig. 6h, the capacitive charge of C@NiO@NC increases from 50.2% to 81.5% as scan rates increase from 0.4 to 4 mV s^{-1}, much higher than that of C@NiO (capacitive charge increases from 36.3% to 65.4%). In particular, when the scan rate is 0.8 mV s^{-1}, the capacitive charge (shaded area) of C@NiO@NC (61.7%) is much higher than that of C@NiO (49.5%), suggesting sandwich-like structure can greatly increase the lithiation kinetics, resulting in better reversibility at high rates (Fig. 6c and f).

To deeply study the effect of N-doped carbon layer for reaction kinetics, DFT calculations were carried out to further reveal the electronic conductivity and Li^+ adsorption energy owing to the presence of N-doped carbon. Calculated density of states (DOS) of pristine NiO show the absence of band gap (Fig. 7a), suggesting that NiO possesses intrinsic metallic property. However, the intensity of DOS between conduction band and valence band is low, indicating the poor electronic conductivity of NiO. After combining NiO and carbon (C or NC), the intensity of DOS at fermi level becomes much higher. For comparison, the intensity of DOS for NiO-NC exhibits the highest value among all structures, indicating the best electronic conductivity of NiO-NC[46, 48]. Differential charge density of NiO−C and NiO-NC are shown in Fig. 7b and d. In detail, differential charge density of NiO-NC at N doped site (dashed rectangle) migrates from N-doped side to NiO side, which is much obvious than that of NiO−C. As a result, NiO surface would accumulate electrons from N-doped carbon, inducing the charge redistributing between NiO and N-doped carbon. This electron accumulation would strongly attract Li^+ in NiO-NC. The computed Li^+ intercalation models for pristine NiO and NiO−C show much more serious volume expansion than that of NiO-NC (Fig. 7c, e and S6), in agreement with the structural stability of NiO-NC mentioned above. The calculation results of Li^+ adsorption energy is depicted in Fig. 7f. Obviously, Li^+ adsorption energy of NiO-NC (−7.831 eV) is calculated to be the lowest among those three models, suggesting better ability for NiO-NC to adsorb Li^+. The detailed calculation results are concluded in Table S2, which can well support the fact that NiO-NC is more favorable for the adsorption of Li^+ under the assistance of N-doped carbon, thus enabling fast reaction kinetics.

4. Conclusions

In summary, we successfully designed and prepared a sandwich-like dual carbon layers coated hollow structured C@NiO@NC. Such structure consists of inside carbon layer, middle NiO nanosheets and outside N-doped carbon layer. This unique hollow structure with high surface area gave rise to efficient contact between the electrode and electrolyte, resulting in shortened ion diffusion pathway. The dual coated carbon layers largely

enhanced the electronic conductivity of NiO and effectively confined the structure variation of NiO during the cycling. When used as an anode material for LIBs, the C@NiO@NC exhibited outstanding cycling stability with a high capacity retention (96.1% at 1000 mA g^{-1} after 1000 cycles) as well as superior rate capability (420 mA h g^{-1} at ultrahigh rate of 10000 mA g^{-1}), which is much better than its counterparts. Theoretical analysis demonstrated the increased electronic conductivity for C@NiO@NC is due to the charge redistribution at the heterointerfaces between N-doped carbon and NiO. The outside nitrogen doped carbon layer also endowed C@NiO@NC with more energetic favorable ability to adsorb the Li^+, resulting in accelerating reaction kinetics. The present preparation method for sandwich-like dual carbon layers coated hollow structure is facile and highly efficient, which can be extended to various transition-metal oxides (FeO_x, CoO_x, SnO_x and etc.) with increased electrochemical performance.

Declaration of competing interest

The authors declare that they have no known competing financial interests or personal relationships that could have appeared to influence the work reported in this paper.

CRediT authorship contribution statement

Qingmeng Gan: Conceptualization, Data curation, Investigation, Writing - original draft. **Buchen Wu:** Conceptualization, Data curation, Investigation, Writing - original draft. **Ning Qin:** Methodology. **Jiali Chen:** Software, Formal analysis. **Wen Luo:** Investigation. **Dejun Xiao:** Conceptualization, Writing - review & editing. **Jie Feng:** Conceptualization, Writing - review & editing. **Youhuan Zhu:** Investigation. **Peisen Zhang:** Writing - review & editing.

Acknowledgement

This research was financially supported by the National Nature Science Foundation of China (No.21671200 and No.21571189).

Appendix A. Supplementary data

Supplementary data to this article can be found online at https://doi.org/10.1016/j.electacta.2020.136121.

References

[1] S. Zhang, Z. Zhang, J. Kang, Q. Huang, Z. Yu, Z. Qiao, Y. Deng, J. Li, W. Wang, Double-shelled nanoporous nio nanocrystal doped MnO/Ni network for high performance lithium-ion battery, Electrochim. Acta 320 (2019) 134542.
[2] S.-K. Park, J.H. Choi, Y.C. Kang, Unique hollow nio nanooctahedrons fabricated through the kirkendall effect as anodes for enhanced lithium-ion storage, Chem. Eng. J. 354 (2018) 327–334.
[3] M.S. Jo, S. Ghosh, S.M. Jeong, Y.C. Kang, J.S. Cho, Coral-like yolk–shell-structured nickel oxide/carbon composite microspheres for high-performance li-ion storage anodes, Nano-Micro Lett. 11 (2019) 3.
[4] W. Yao, S. Wu, L. Zhan, Y. Wang, Two-dimensional porous carbon-coated sandwich-like mesoporous SnO_2/graphene/mesoporous SnO_2 nanosheets towards high-rate and long cycle life lithium-ion batteries, Chem. Eng. J. 361 (2019) 329–341.
[5] P. Bhattacharya, J.H. Lee, K.K. Kar, H.S. Park, Carambola-shaped SnO_2 wrapped in carbon nanotube network for high volumetric capacity and improved rate and cycle stability of lithium ion battery, Chem. Eng. J. 369 (2019) 422–431.
[6] L. Yin, Y.J. Gao, I. Jeon, H. Yang, J.-P. Kim, S.Y. Jeong, C.R. Cho, Rice-panicle-like γ-Fe_2O_3@C nanofibers as high-rate anodes for superior lithium-ion batteries, Chem. Eng. J. 356 (2019) 60–68.
[7] Q. Zhao, J. Liu, X. Li, Z. Xia, Q. Zhang, M. Zhou, W. Tian, M. Wang, H. Hu, Z. Li, W. Wu, H. Ning, M. Wu, Graphene oxide-induced synthesis of button-shaped amorphous Fe_2O_3/rGO/CNFs films as flexible anode for high-performance lithium-ion batteries, Chem. Eng. J. 369 (2019) 215–222.
[8] X. Yin, C. Zhi, W. Sun, L.-P. Lv, Y. Wang, Multilayer NiO@Co_3O_4@graphene quantum dots hollow spheres for high-performance lithium-ion batteries and supercapacitors, J. Mater. Chem. 7 (2019) 7800–7814.
[9] D. Guo, L. Pan, J. Hao, L. Han, D. Yi, Y. Wang, Y. Yang, B. Yoshio, X. Wang, Nanosheets-in-nanotube Co_3O_4-carbon array design enables stable Li-ion storage, Carbon 147 (2019) 501–509.
[10] Y. Feng, H. Zhang, W. Li, L. Fang, Y. Wang, Targeted synthesis of novel hierarchical sandwiched NiO/C arrays as high-efficiency lithium ion batteries anode, J. Power Sources 301 (2016) 78–86.
[11] X. Zheng, H. Wang, C. Wang, Z. Deng, L. Chen, Y. Li, T. Hasan, B.-L. Su, 3D interconnected macro-mesoporous electrode with self-assembled NiO nanodots for high-performance supercapacitor-like Li-ion battery, Nanomater. Energy 22 (2016) 269–277.
[12] J. Zhang, W. Luo, T. Xiong, R. Yu, P. Wu, J. Zhu, Y. Dai, L. Mai, Carboxyl functionalized carbon incorporation of stacked ultrathin NiO nanosheets: topological construction and superior lithium storage, Nanoscale 11 (2019) 7588–7594.
[13] S. Hwan Oh, J.-S. Park, M. Su Jo, Y.C. Kang, J.S. Cho, Design and synthesis of tube-in-tube structured NiO nanobelts with superior electrochemical properties for lithium-ion storage, Chem. Eng. J. 347 (2018) 889–899.
[14] H. Pang, B. Guan, W. Sun, Y. Wang, Metal-organic-frameworks derivation of mesoporous NiO nanorod for high-performance lithium ion batteries, Electrochim. Acta 213 (2016) 351–357.
[15] J. Tian, Q. Shao, X. Dong, J. Zheng, D. Pan, X. Zhang, H. Cao, L. Hao, J. Liu, X. Mai, Z. Guo, Bio-template synthesized NiO/C hollow microspheres with enhanced Li-ion battery electrochemical performance, Electrochim. Acta 261 (2018) 236–245.
[16] H. He, Q. Gan, H. Wang, G.-L. Xu, X. Zhang, D. Huang, F. Fu, Y. Tang, K. Amine, M. Shao, Structure-dependent performance of TiO_2/C as anode material for Na-ion batteries, Nanomater. Energy 44 (2018) 217–227.
[17] X. Li, Z. Zhang, J. Li, Y. Ma, Y. Qu, Structural influence of porous FeO_x@C nanorods on their performance as anodes of lithium-ion batteries, J. Mater. Chem. 3 (2015) 18649–18656.
[18] G. Zhang, S. Hou, H. Zhang, W. Zeng, F. Yan, C.C. Li, H. Duan, High-performance and ultra-stable lithium-ion batteries based on MOF-derived ZnO@ZnO quantum dots/C core-shell nanorod arrays on a carbon cloth anode, Adv. Mater. 27 (2015) 2400–2405.
[19] Q. Gan, H. He, K. Zhao, Z. He, S. Liu, Preparation of N-doped porous carbon coated MnO nanospheres through solvent-free in-situ growth of ZIF-8 on $ZnMn_2O_4$ for high-performance lithium-ion battery anodes, Electrochim. Acta 266 (2018) 254–262.
[20] Q. Gan, K. Zhao, S. Liu, Z. He, Solvent-free synthesis of N-doped carbon coated ZnO nanorods composite anode via a ZnO support-induced ZIF-8 in-situ growth strategy, Electrochim. Acta 250 (2017) 292–301.
[21] Q. Wang, R. Zou, W. Xia, J. Ma, B. Qiu, A. Mahmood, R. Zhao, Y. Yang, D. Xia, Q. Xu, Facile synthesis of ultrasmall CoS_2 nanoparticles within thin N-doped porous carbon shell for high performance lithium-ion batteries, Small 11 (2015) 2511–2517.
[22] L. Xia, S. Wang, G. Liu, L. Ding, D. Li, H. Wang, S. Qiao, Flexible SnO_2/N-doped carbon nanofiber films as integrated electrodes for lithium-ion batteries with superior rate capacity and long cycle life, Small 12 (2016) 853–859.
[23] Y. Feng, H. Zhang, Y. Zhang, Y. Bai, Y. Wang, Novel peapod NiO nanoparticles encapsulated in carbon fibers for high-efficiency supercapacitors and lithium-ion batteries, J. Mater. Chem. 4 (2016) 3267–3277.
[24] Q. Gan, H. He, K. Zhao, Z. He, S. Liu, Morphology-dependent electrochemical performance of Ni-1, 3, 5-benzenetricarboxylate metal-organic frameworks as an anode material for Li-ion batteries, J. Colloid Interface Sci. 530 (2018) 127–136.
[25] J. Liang, H. Hu, H. Park, C. Xiao, S. Ding, U. Paik, X.W. Lou, Construction of hybrid bowl-like structures by anchoring NiO nanosheets on flat carbon hollow particles with enhanced lithium storage properties, Energy Environ. Sci. 8 (2015) 1707–1711.
[26] C. Lei, F. Han, D. Li, W.C. Li, Q. Sun, X.Q. Zhang, A.H. Lu, Dopamine as the coating agent and carbon precursor for the fabrication of N-doped carbon coated Fe_3O_4 composites as superior lithium ion anodes, Nanoscale 5 (2013) 1168–1175.
[27] Y. Zhang, Y.V. Lim, S. Huang, M.E. Pam, Y. Wang, L.K. Ang, Y. Shi, H.Y. Yang, Tailoring NiO nanostructured arrays by sulfate anions for sodium-ion batteries, Small 14 (2018) 1800898.
[28] S.I. Kim, J.S. Lee, H.J. Ahn, H.K. Song, J.H. Jang, Facile route to an efficient NiO supercapacitor with a three-dimensional nanonetwork morphology, ACS Appl. Mater. Interfaces 5 (2013) 1596–1603.
[29] Y. Xiao, X. Wang, W. Wang, D. Zhao, M. Cao, Engineering hybrid between MnO and N-doped carbon to achieve exceptionally high capacity for lithium-ion battery anode, ACS Appl. Mater. Interfaces 6 (2014) 2051–2058.
[30] Y. Yang, X. Ji, M. Jing, H. Hou, Y. Zhu, L. Fang, X. Yang, Q. Chen, C.E. Banks, Carbon dots supported upon N-doped TiO_2 nanorods applied into sodium and lithium ion batteries, J. Mater. Chem. 3 (2015) 5648–5655.
[31] Z. Qiu, Y. Lin, H. Xin, P. Han, D. Li, B. Yang, P. Li, S. Ullah, H. Fan, C. Zhu, J. Xu, Ultrahigh level nitrogen/sulfur co-doped carbon as high performance anode materials for lithium-ion batteries, Carbon 126 (2018) 85–92.
[32] L. Zhang, J. Yue, T. Wei, Z. Liu, J. Zhou, C. Liu, H. Jiang, Z. Jiang, Z. Fan, Densely pillared holey-graphene block with high-level nitrogen doping enabling ultrahigh volumetric capacity for lithium ion storage, Carbon 142 (2019) 327–336.
[33] Y.F. Li, Y.H. Shi, S.G. Wang, J.H. Liu, J. Lin, Y. Xia, X.L. Wu, C.Y. Fan, J.P. Zhang, H.M. Xie, H.Z. Sun, Z.M. Su, Carbon/binder-free NiO@NiO/NF with in situ formed interlayer for high-areal-capacity lithium storage, Adv. Energy Mater. 9 (2019) 1803690.

[34] Q. Gan, H. He, K. Zhao, Z. He, S. Liu, S. Yang, Plasma-induced oxygen vacancies in urchin-like anatase titania coated by carbon for excellent sodium-ion battery anodes, ACS Appl. Mater. Interfaces 10 (2018) 7031–7042.
[35] H. He, D. Sun, Y. Tang, H. Wang, M. Shao, Understanding and improving the initial coulombic efficiency of high-capacity anode materials for practical sodium ion batteries, Energy Storage Materials 23 (2019) 233–251.
[36] Z. Fan, J. Liang, W. Yu, S. Ding, S. Cheng, G. Yang, Y. Wang, Y. Xi, K. Xi, R.V. Kumar, Ultrathin NiO nanosheets anchored on a highly ordered nanostructured carbon as an enhanced anode material for lithium ion batteries, Nanomater. Energy 16 (2015) 152–162.
[37] W. Yang, G. Cheng, C. Dong, Q. Bai, X. Chen, Z. Peng, Z. Zhang, NiO nanorod array anchored Ni foam as a binder-free anode for high-rate lithium ion batteries, J. Mater. Chem. 2 (2014) 20022–20029.
[38] D. Xu, C. Mu, B. Wang, J. Xiang, W. Ruan, F. Wen, X. Du, Z. Liu, Y. Tian, Fabrication of multifunctional carbon encapsulated Ni@NiO nanocomposites for oxygen reduction, oxygen evolution and lithium-ion battery anode materials, Sci. China Mater. 60 (2017) 947–954.
[39] J. Li, D. Yan, S. Hou, T. Lu, Y. Yao, D.H.C. Chua, L. Pan, Metal-organic frameworks derived yolk-shell ZnO/NiO microspheres as high-performance anode materials for lithium-ion batteries, Chem. Eng. J. 335 (2018) 579–589.
[40] D. Su, M. Ford, G. Wang, Mesoporous NiO crystals with dominantly exposed {110} reactive facets for ultrafast lithium storage, Sci. Rep. 2 (2012) 924.
[41] H.S. Jadhav, G.M. Thorat, J. Mun, J.G. Seo, Self-assembled hierarchical 3D-NiO microspheres with ultra-thin porous nanoflakes for lithium-ion batteries, J. Power Sources 302 (2016) 13–21.
[42] H. He, D. Huang, W. Pang, D. Sun, Q. Wang, Y. Tang, X. Ji, Z. Guo, H. Wang, Plasma-induced amorphous shell and deep cation-site S doping endow TiO_2 with extraordinary sodium storage performance, Adv. Mater. 30 (2018) 1801013.
[43] Y. Liu, Z. Chen, H. Jia, H. Xu, M. Liu, R. Wu, Iron-doping-induced phase transformation in dual-carbon-confined cobalt diselenide enabling superior lithium storage, ACS Nano 13 (2019) 6113–6124.
[44] C. Chen, Z. Wang, B. Zhang, L. Miao, J. Cai, L. Peng, Y. Huang, J. Jiang, Y. Huang, L. Zhang, J. Xie, Nitrogen-rich hard carbon as a highly durable anode for high-power potassium-ion batteries, Energy Storage Materials 8 (2017) 161–168.
[45] G. Zou, C. Wang, H. Hou, C. Wang, X. Qiu, X. Ji, Controllable interlayer spacing of sulfur-doped graphitic carbon nanosheets for fast sodium-ion batteries, Small 13 (2017) 1700762.
[46] Q. Gan, J. Xie, Y. Zhu, F. Zhang, P. Zhang, Z. He, S. Liu, Sub-20 nm carbon nanoparticles with expanded interlayer spacing for high-performance potassium storage, ACS Appl. Mater. Interfaces 11 (2019) 930–939.